

REDUCTION OF AERODYNAMIC HEATING AND DRAG WITH OPPOSING JET THROUGH EXTENDED NOZZLE IN HIGH ENTHALPY FLOW

Naoki Morimoto*, Shigeru Aso* , Yasuhiro Tani*
*Kyushu University, Fukuoka, Japan

Keywords: *Thermal protection, Drag reduction, Opposing jet through extended nozzle, Hypersonic, High enthalpy flow*

Abstract

The experimental and numerical investigations of an opposing jet through an extended nozzle are described. The opposing jet through the extended nozzle is a new type of thermal protection devices combining an opposing jet and a forward facing spike. The experimental measurements of the heat flux distribution on a hemispherical-cylindrical blunt test model were conducted in a free piston shock tunnel in Kyushu University. The present test flow condition is 5,600 m/s and Mach number at 6.6. The shock tunnel testing demonstrates capabilities of this device reducing the heat flux up to 92% in hypersonic and high enthalpy flow. In addition, axisymmetric Navier-Stokes numerical simulations were carried out. The numerical simulations show reduction of both aerodynamic heating and drag with precise explanations of the flow field structure.

1 Introduction

Reducing both aerodynamic heating and drag is one of the most difficult design requirements for hypervelocity vehicles. To deal with this problem, many researchers have proposed various active thermal protection systems (TPS) like an opposing jet[1][2] or a forward facing spike[3]. The performance of these devices is almost proportional trend to the total pressure of an opposing jet and the length of a spike. If a designer tries to employ those devices, TPS weight including coolant gases could become heavy with increas-

ing flight Mach number. Practically, the lighter TPS is the better for applications in the future hypervelocity flight vehicles.

The idea combining the spike with a gas ejection has been brought to enhance TPS performance. Reding and Jecmen[4] burned hydrogen in a region of spike-induced separated flow. This experimental study showed that the external burning reduces aerodynamic drag below that achievable with an ordinary spike. Jiang et al.[5] introduced lateral jets from the tip of the spike. This lateral jet pushes the conical shock wave originating from the tip of the spike away from the blunt body, so that it reduces the peak value of pressure and heat flux around the reattachment point. Tamada et al.[6] proposed the opposing jet through an extended nozzle and demonstrated its performance by CFD analysis. The shape of this device is similar to “blowpipes” used by glass blowers. The extended nozzle is intended for the purpose of enlarging the recirculation region even by weak opposing jet. The flow fields with some TPS’s are compared in Fig.1.

As far as the present authors have surveyed the literatures, no study could be found dealing with the opposing jet through the extended nozzle in high enthalpy hypersonic flow. In the present paper, a shock tunnel test campaign shows the capability to alleviate aerodynamic heating by the opposing jet through the extended nozzle. In addition, CFD simulations describe the performance reducing both aerodynamic heating and drag with precise explanations of the flow field.

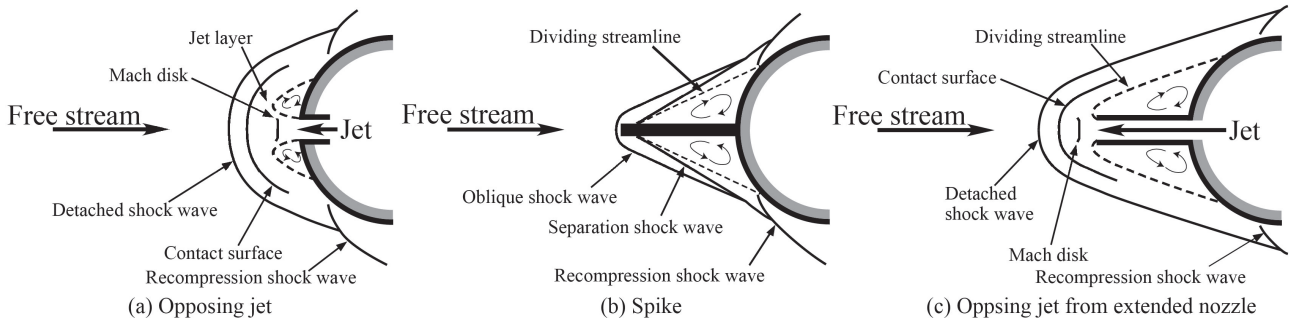


Fig. 1 Flow fields around active TPS.

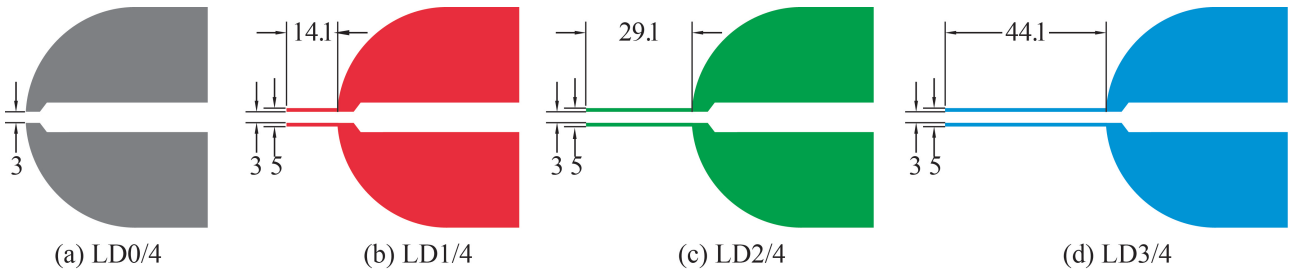


Fig. 2 Variation of extended nozzles, units in mm.

2 Test Methodologies

2.1 Test Model

Test models are shown in Fig.2. The hemispherical cylindrical blunt test models were used. These models are 60 mm in diameter and have nozzles at the nose to eject the coolant gas. The length of the extended nozzle is 0 mm, 14.1 mm, 29.1 mm, or 44.1 mm. These models were named “LD0/4”, “LD1/4”, “LD2/4”, and “LD3/4”, respectively. Each extended nozzle is 5 mm in outer diameter and 3 mm in inner diameter.

Experimental and numerical studies were conducted with varying (1) the length of the extended nozzle and (2) the total pressure of the opposing jet. Mach number of the opposing jet was unity at the nozzle exit.

2.2 Experimental Study

The shock tunnel experiments were conducted in a free piston shock tunnel in Kyushu University. The conical nozzle of the shock tunnel is 10° in the half angle and 270 mm in the exit diameter. The test gas was air. The free stream velocity,

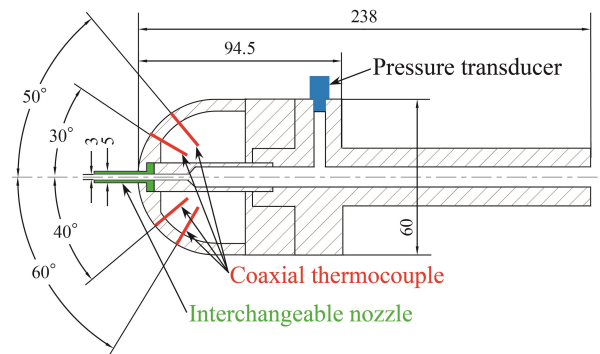


Fig. 3 Schematic of test model, units in mm.

static temperature, static pressure, Mach number, and Reynolds number per unit meter were 5,600 m/s, 1,100 K, 440 Pa, 6.6, 1.1×10^5 1/m, respectively. These properties were estimated by CEA[7] and NENZF[8] programs. The shock tunnel was operated on a tuned piston operation and a tailored interface condition to maximize test time. The test time in the shock tunnel was typically 100 μ s.

The schematic of the test model is shown in Fig.3. The extended nozzles are interchangeable.

REDUCTION OF AERODYNAMIC HEATING AND DRAG WITH OPPOSING JET THROUGH EXTENDED NOZZLE IN HIGH ENTHALPY FLOW

The surface temperature histories on 30°, 40°, 50° and 60° from central axis were measured by E-type coaxial thermocouples (MEDTHERM TCS-10370). The coolant gas for the opposing jet was nitrogen in the present study. The coolant gas was provided from a gas reservoir located outside of the shock tunnel. The total pressure of the opposing jet was 40 kPa or 80 kPa. Each test case was repeated at least twice for precise measurement.

The test results were reduced in a Stanton number. The heat flux was calculated from the temperature histories measured within the test duration time from Eq. (1). This method is popular in short duration shock tunnel facilities.

$$q_{\text{wall}}(t_n) = 2\sqrt{\frac{\rho c k}{\pi}} \sum_{i=1}^n \frac{T_{\text{wall}}(t_i) - T_{\text{wall}}(t_{i-1})}{\sqrt{t_n - t_i} + \sqrt{t_n - t_{i-1}}} \quad (1)$$

where q , t , $\sqrt{\rho c k}$, and T denote the heat flux, time, wall material value, and temperature, respectively. Then the Stanton number C_H is

$$C_H = \frac{q_{\text{wall}}}{\rho_{\infty} u_{\infty} c_{p\infty} (T_{aw} - T_{\text{wall}})} \quad (2)$$

where ρ_{∞} , u_{∞} , and $c_{p\infty}$ denote the density, velocity, and specific heat at constant pressure of the test flow. The adiabatic wall temperature T_{aw} in laminar flows is defined as follows:

$$T_{aw} = T_{\infty} \left(1 + \sqrt{Pr_{\infty}} \frac{\gamma - 1}{2} M_{\infty}^2\right). \quad (3)$$

2.3 Numerical Study

In the present CFD study, the gases in both the test flow and the opposing jet were regarded as the perfect gas of air. The test flow conditions are the same as that of the experimental study. The finite difference method was used with axisymmetric Navier-Stokes equations. The inviscid term was calculated by AUSM_DV scheme with MUSCL interpolation. The viscous term was computed by spatially second-order central difference method. The time integration was made by LU-ADI factorization algorithm. Though the flow field around the opposing jet contains shear layers and boundary layers, no turbulence

model was employed in the present study because Reynolds number based on the model diameter is small enough: that is 6,600. The total pressure of the opposing jet was varied from 40 kPa to 80 kPa every 10 kPa. The number of structured grid points was 240,000 for each case. The minimum height of the grid near the model wall was 10^{-5} m. The grid arrangements were clustered around the nozzle edge and the area which was assumed to contain shock-shock interactions. The boundary conditions of the model wall were non-slip and isothermal at 300 K.

The heat flux on the model wall was calculated by the temperature gradient near the wall. The thermal conductivity for each grid point was estimated with the Chapman-Enskog theory.

A total heat load was calculated by this equation:

$$Q = 2\pi \int_{\text{wall}} q_{\text{wall}} r ds \quad (4)$$

where Q , r , and ds denotes the total heat load, local radius, and control length, respectively. The heat flux on the extended nozzle was also included in Eq.(4). Note that the heat flux in the region toward larger diameters of the blunt body is dominant in Eq.(4) because the surface area $2\pi r ds$ of such region becomes large for a certain ds .

The aerodynamic drag was calculated by Eq.(5).

$$\text{Drag} = F_{\text{pressure}} + F_{\text{shear stress}} + F_{\text{jet thrust}} \quad (5)$$

where

$$F_{\text{pressure}} = 2\pi \int_{\text{wall}} p_{\text{wall}} \sin \theta r ds \quad (6)$$

$$F_{\text{shear stress}} = 2\pi \int_{\text{wall}} \tau_{\text{wall}} \cos \theta r ds \quad (7)$$

$$F_{\text{jet thrust}} = \rho_{j,\text{exit}} u_{j,\text{exit}}^2 + (p_{j,\text{exit}} - p_{0,2}) A_{j,\text{exit}} \quad (8)$$

where F , p , θ denotes the force, local pressure, and the angle between free stream and body tangent, respectively. The shear stress τ was calculated as the product of the viscosity and the velocity gradient on the model wall. The viscosity for each grid point was estimated with Sutherland's equation. The pressure and the shear stress on the extended nozzle are also included.

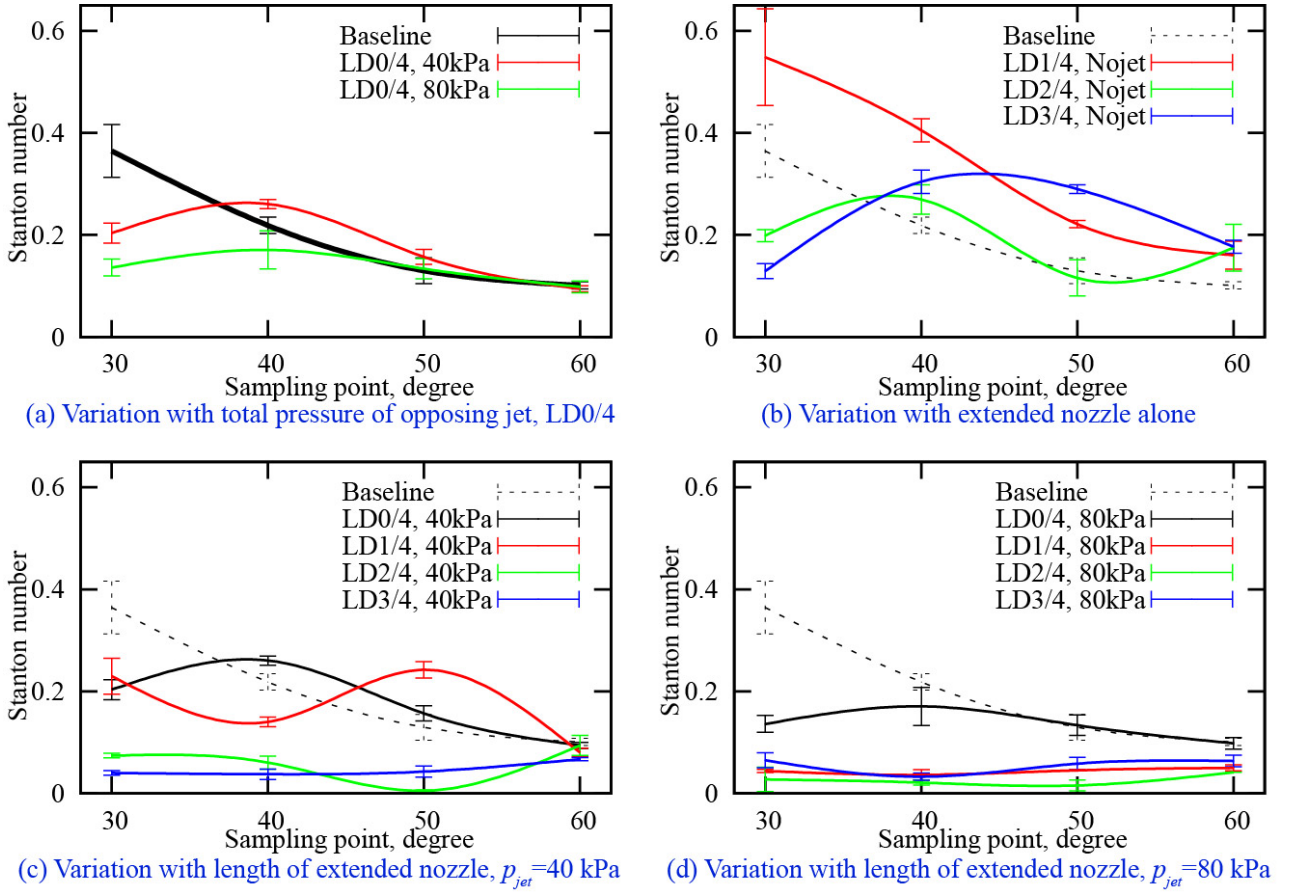


Fig. 4 Distributions of experimentally measured Stanton number.

3 Results and Discussions

3.1 Experimental Measurements of Aerodynamic Heating

The experimental results are shown in Fig.4. Error bars presented here are based on 2σ of the measurements, where σ is a standard deviation. The changes in the heat flux distribution solely by the opposing jet are shown in Fig.4(a). The Stanton number distribution indicated as “Baseline” stands for the case of LD0/4 without the opposing jet. The heat flux only in the vicinity of the stagnation point reduced by both conditions of the opposing jet. The thermal protection effects solely by the extended nozzle are shown in Fig.4(b). The extended nozzle for these conditions can be regarded as the spike. The Stanton number for LD1/4 increased at all measuring points compared with the baseline. When LD2/4 and LD3/4 model were used, the Stanton number

at 30° decreased 46 % and 65 %, respectively; however, the Stanton number between 40° and 60° were increased or almost the same. The thermal protection effects by the combinational device are shown in Fig.4(c) and (d). When the opposing jet with total pressure of 40 kPa was used, the Stanton number at 30° and 40° of LD1/4 decreased about 30%. In comparison with LD0/4 at the same jet condition, the peak position of the Stanton number shifted from 40° to 50° . This fact suggests that the reattachment point moved downstream due to the addition of the extended nozzle. On the other hand, the Stanton number for LD2/4 and LD3/4 model decreased at every measuring point. This reduction of the Stanton number was more successful than that of LD0/4 with the total pressure of 80 kPa. These results indicate that the extended nozzle reduces mass flow of the opposing jet required to attain thermal protection. When the opposing jet with the total pressure of 80 kPa was used, significant reduc-

REDUCTION OF AERODYNAMIC HEATING AND DRAG WITH OPPOSING JET THROUGH EXTENDED NOZZLE IN HIGH ENTHALPY FLOW

tion of the heat flux was observed for all results with the extended nozzle.

3.2 Numerical Simulations

3.2.1 Flow Field

Throughout this section, suppose that all properties are time averaged because of flow instabilities. The time averaged simulated flow fields are shown in Fig.5. In addition, the locations of the flow reattachment to the model wall are listed in Table.1. These reattachment points are judged from the shear stress on the model wall. The shock wave detachment distance of the baseline case, shown in Fig.5(a), agreed within 3% with the empirical formula of Billig[9]. Because the energy relaxation by the chemical reactions was not included in the present simulation, the temperature behind the bow shock wave exceeded 10,000 K.

In the cases of the opposing jet and/or the extended nozzle, the recirculating region was formed around the stagnation point. The plural vortices can be observed in each recirculation region. The recirculation region became large with either the stronger opposing jet or the longer extended nozzle. Moreover, the flow field in front of the test model changed from that of a blunt body to that of a slender body. The thickness of the jet layer covering on the test model increased with an increase in the total pressure of the opposing jet.

According to Edney's classification of shock-shock interactions[10], the interaction of LD1/4 without the opposing jet was "Mode V" and those

of LD2/4 and LD3/4 without the opposing jet were "Mode VI". Judging from the shock-shock interactions, LD1/4 model without the opposing jet is unsuitable for a TPS because the heat transfer to the model wall is strengthened under the Mode V interaction.

3.2.2 Heat Load

The heat flux distributions are compared in Fig.6. The heat flux distributions when the opposing jet solely used are shown in Fig.6(a). The heat flux near the stagnation point decreased; however, the heat flux partially rose above the baseline distribution when the opposing jet with the total pressure less than 60 kPa was used. Comparing these distributions with the present experimental measurements, both results qualitatively agreed. The lack of quantitative coincidence of these results seems to be due to the disregard of chemical reactions and radiative heat transfer in the present CFD simulation. The heat flux distributions in the case of LD1/4 are shown in Fig.6(b). The reduction of the heat flux was more significant than that of LD0/4 with the same jet conditions. In contrast, the harsh heat flux was observed at the tip of the extended nozzle and the region between 30° and 40° in the case without the opposing jet. The heat flux distributions in the case of LD2/4 and LD3/4 are shown in Fig.6(c) and (d). The heat flux decreased in similar tendency to the case of LD1/4 except near the peak. The present authors believe that such differences on the shape around the peak are brought by the distinguishable mode change of shock-shock interactions. The common trend for all cases, the peak value of the heat flux existed after the reattachment point. The differences between the peak and the reattachment point were in the range of 5° to 20°. This fact suggests that the recompressing process brings the peak of the heat flux. The high temperature regions by the recompression can be practically observed, for example in Fig.5(a)-(e), (i), and (m).

The total heat load is compared in Fig.7 to evaluate the performance as a TPS. The total heat load decreased in all cases with the opposing jet through the extended nozzle. The reduction rate

Table 1 Reattachment point from simulations.

jet	LD0/4	LD1/4	LD2/4	LD3/4
Nojet	-	33.6°	38.5°	42.6°
40kPa	30.7°	41.1°	47.8°	51.6°
50kPa	32.5°	42.0°	49.2°	52.9°
60kPa	33.0°	42.4°	50.6°	54.0°
70kPa	33.8°	41.8°	50.8°	54.1°
80kPa	33.6°	38.0°	50.8°	53.1°

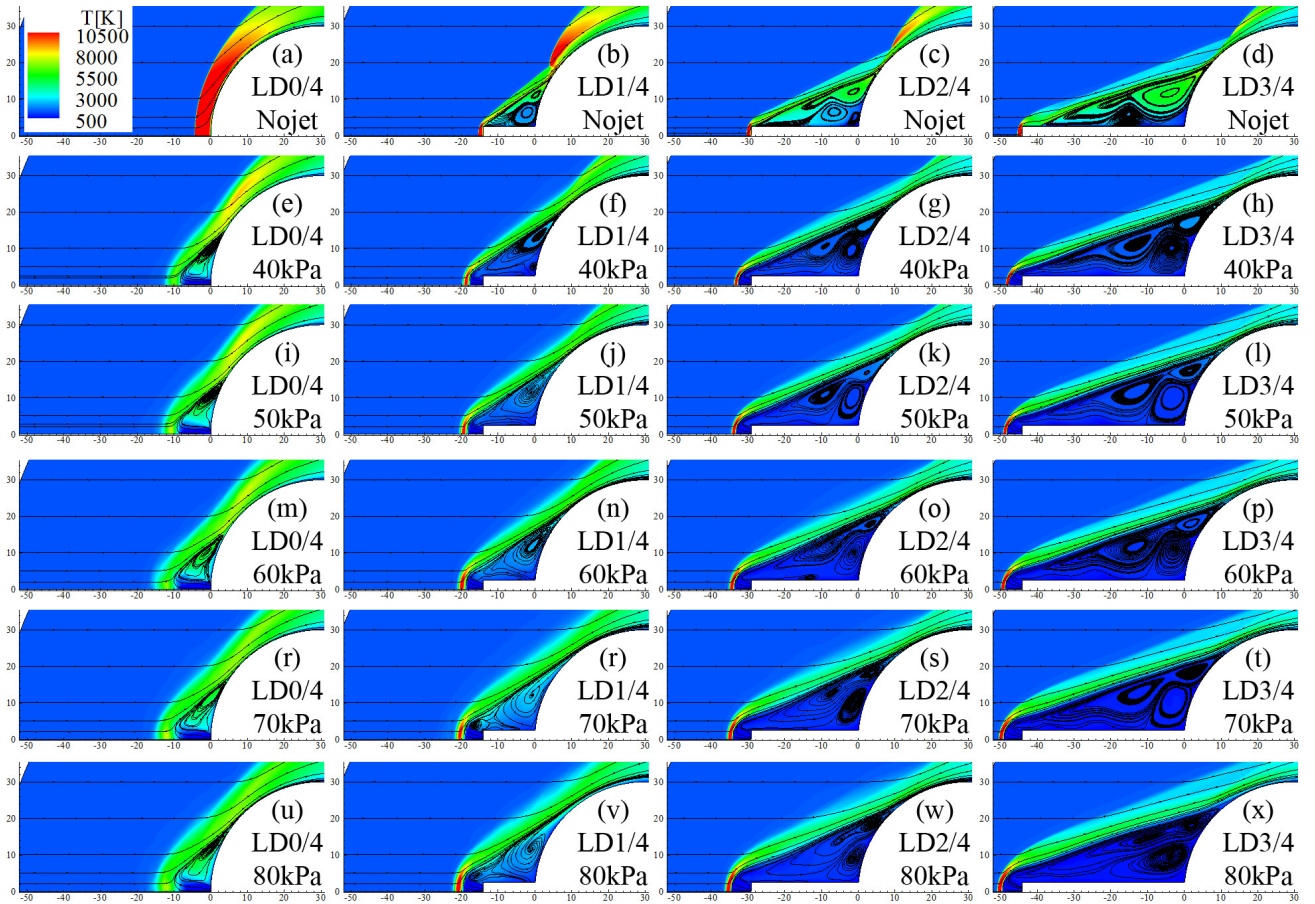


Fig. 5 Time averaged simulated flow fields. Temperature contour and streamline are shown.

were enhanced with relatively strong opposing jet or relatively long extended nozzle. These results suggest that the total heat load decrease monotonically with an increase in the total pressure of the opposing jet. The maximum reduction was 92% in the case of LD3/4 at a jet total pressure of 80 kPa. Though the heat flux only in the vicinity of the stagnation point alleviated by the spike mode, the total heat load on those cases did not decrease.

3.2.3 Aerodynamic Drag

The surface pressure distributions are compared in Fig.8. The pressure decreased by the opposing jet and/or the extended nozzle especially near the stagnation point. The peak value of the pressure existed downstream of the reattachment point in the range of 5° to 10° .

The variations of the simulated aerodynamic drag are shown in Fig.9. The aerodynamic drag

decreased for all cases with the opposing jet through the extended nozzle. The maximum reduction was 70% in the case of LD3/4 at a jet total pressure of 80 kPa. When the device was used as a spike mode, the rate of the drag reduction was smaller than that of the combinational use. Also, when the opposing jet was used solely, the reduction rate was smaller. In the present jet conditions, the simulated drag for LD1/4, LD2/4, and LD3/4 became small with an increase in the jet total pressure; however, the present authors expect an optimum jet condition for the maximum reduction of aerodynamic drag. The main reason for this prospect is the jet thrust itself, which would spoil the reduction of the pressure and viscous drags.

4 Conclusion

The experimental and numerical investigations have been conducted to illustrate the capabilities

REDUCTION OF AERODYNAMIC HEATING AND DRAG WITH OPPOSING JET THROUGH EXTENDED NOZZLE IN HIGH ENTHALPY FLOW

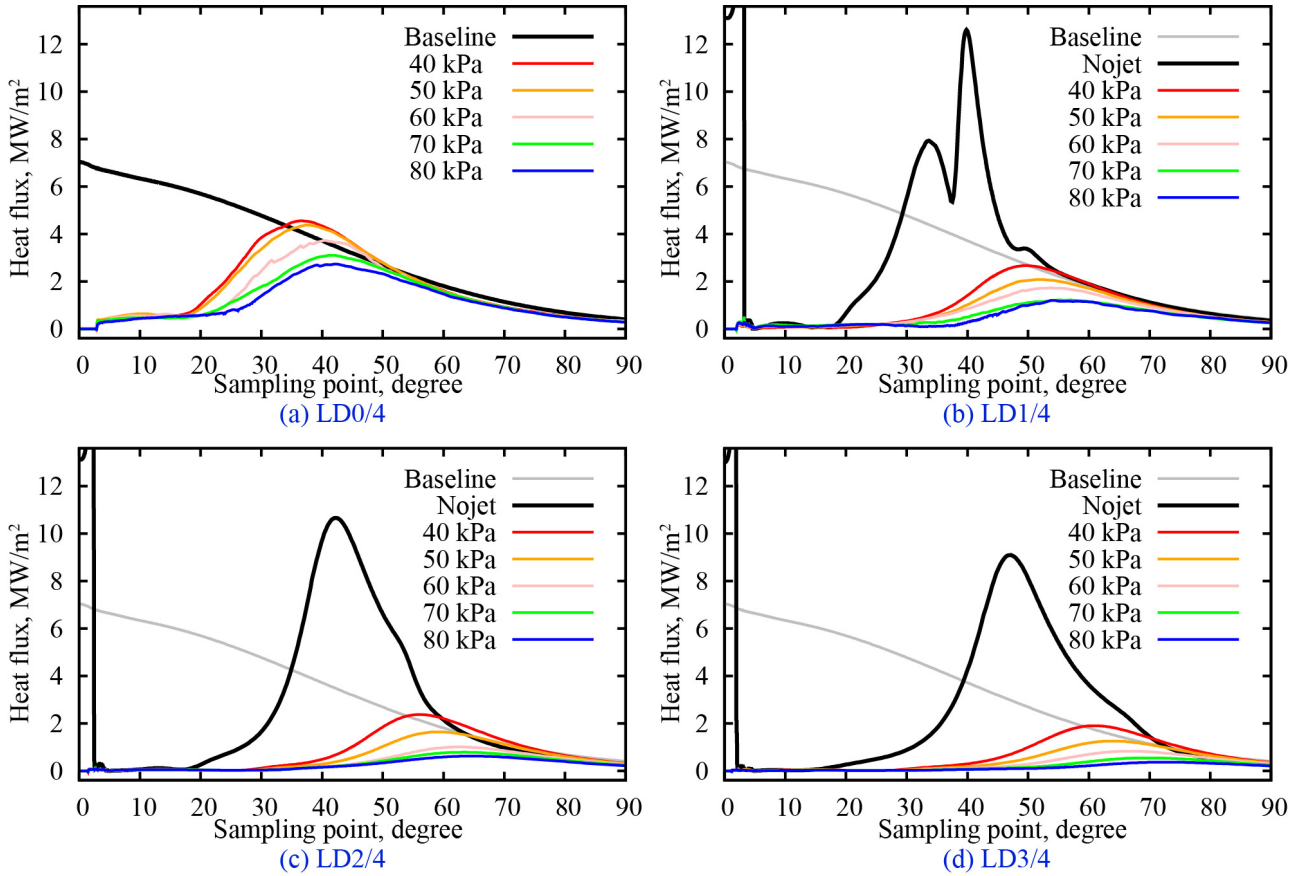


Fig. 6 Simulated surface heat flux distributions.

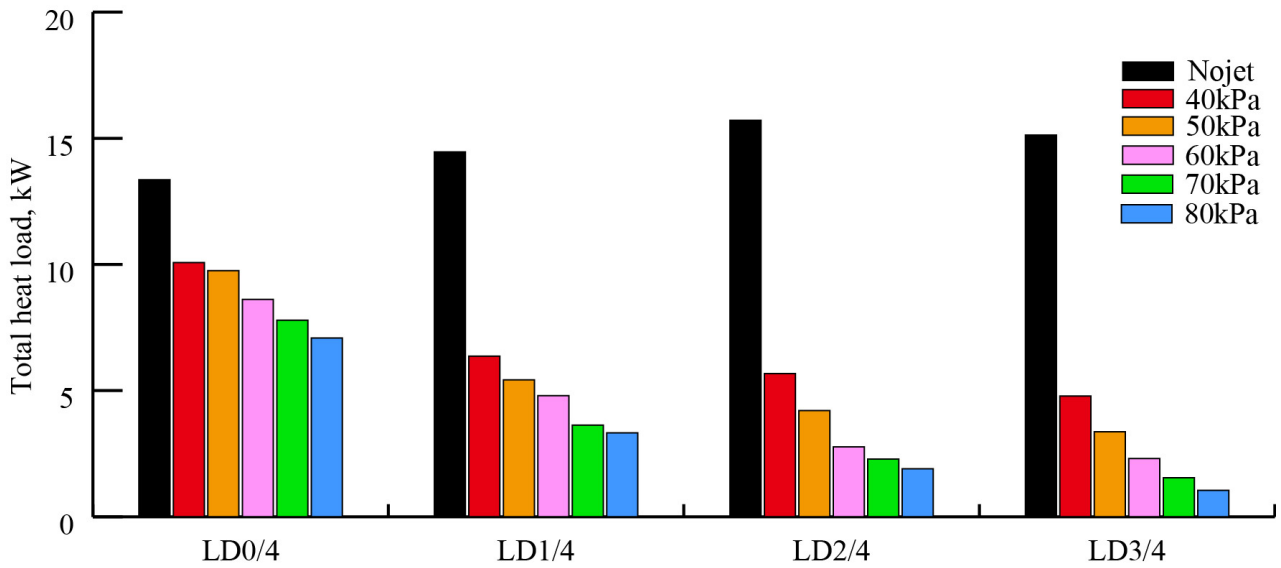


Fig. 7 Variation of total heat load.

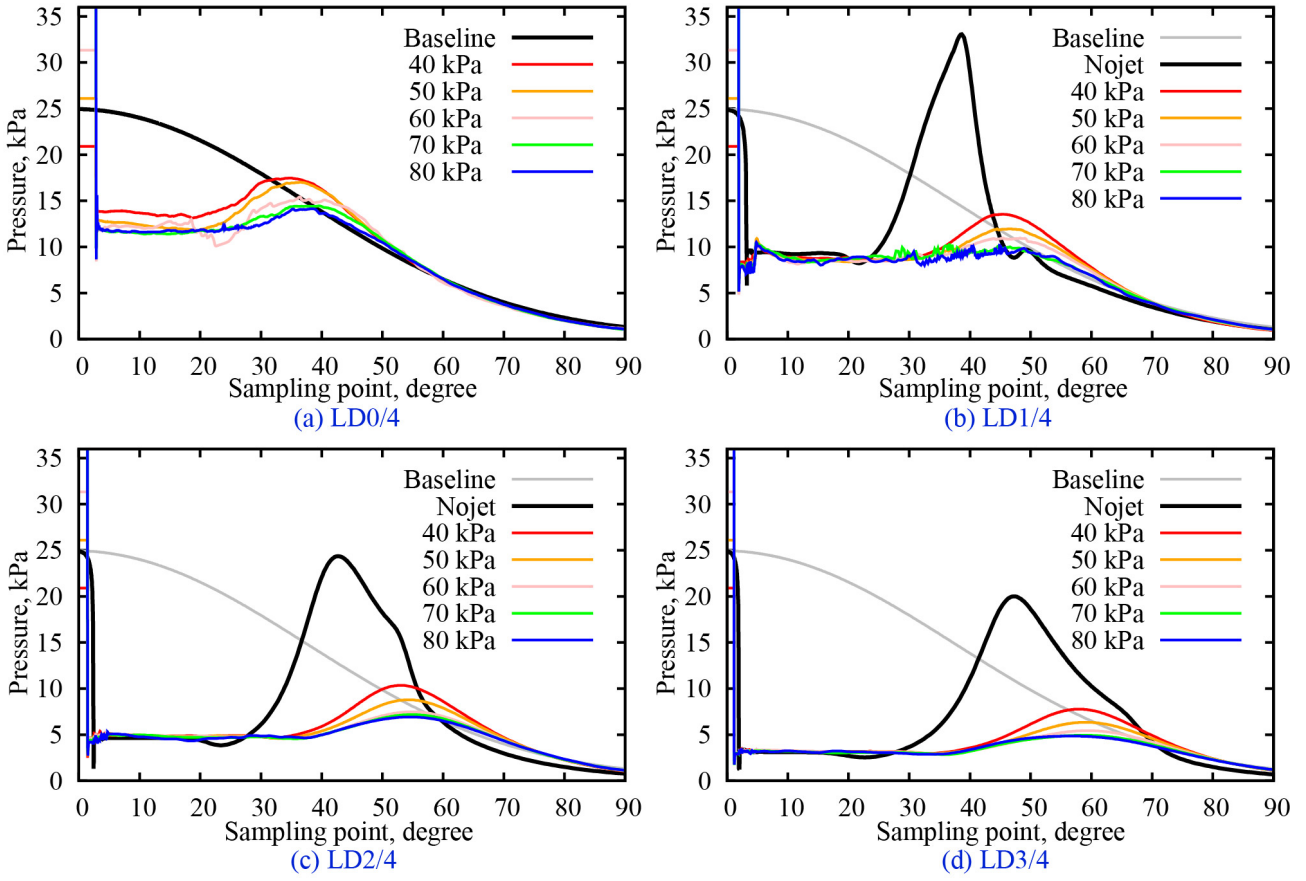


Fig. 8 Simulated surface pressure distributions.

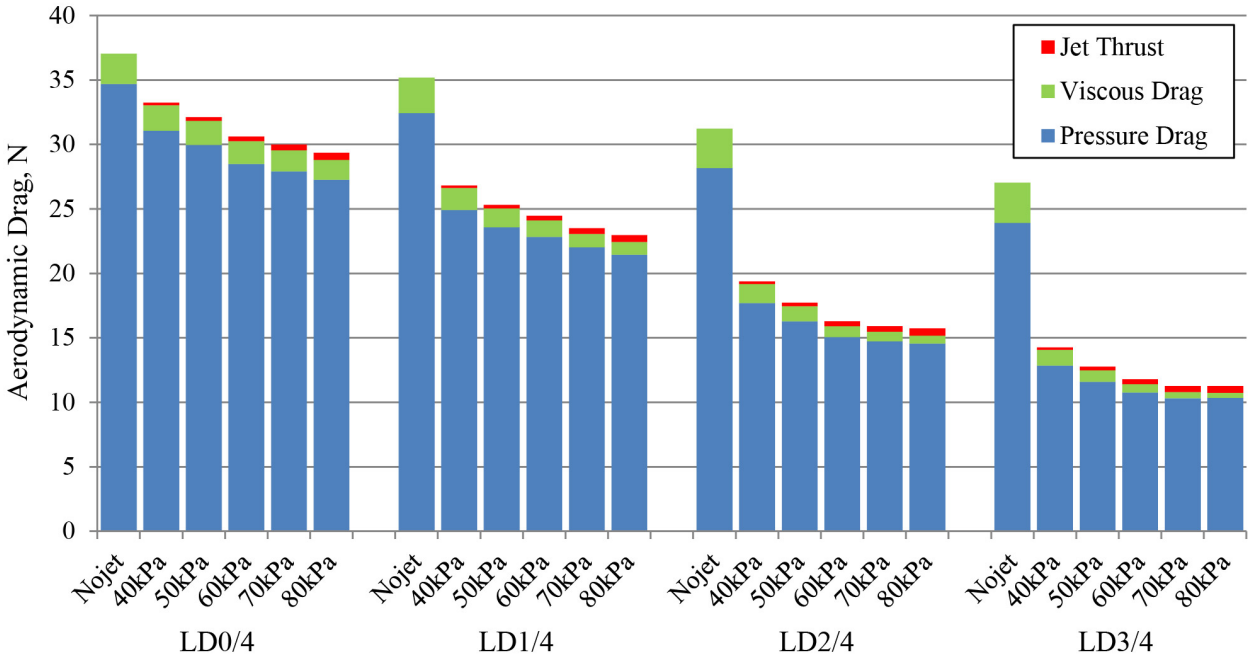


Fig. 9 Variation of aerodynamic drag.

REDUCTION OF AERODYNAMIC HEATING AND DRAG WITH OPPOSING JET THROUGH EXTENDED NOZZLE IN HIGH ENTHALPY FLOW

of reducing both aerodynamic heating and drag. The effects of thermal protection and drag reduction were demonstrated by comparing the distributions of the heat flux and the pressure on the test model.

For the present test conditions, relatively strong opposing jet and relatively long extended nozzle reduces aerodynamic heating and drag simultaneously. Although the reduction of aerodynamic heating could be asymptotic to a certain value, an optimum jet condition for a maximum drag reduction must exist.

References

- [1] Hayashi K, Aso S and Tani Y. Experimental study on thermal protection system by opposing jet in supersonic flow. *Journal of Spacecraft and Rockets*, Vol. 43, No. 1, pp. 233-235, 2006.
- [2] Imoto T, Okabe H, Aso S and Tani Y. Enhancement of aerodynamic heating reduction in high enthalpy flows with opposing jet. *Proc 49th AIAA Aerospace Sciences Meeting and Exhibit*, Orlando, USA, AIAA Paper 2011-0346, 2011.
- [3] Ahmed M and Qin N. Recent advances in the aerothermodynamics of spiked hypersonic vehicles. *Progress in Aerospace Sciences*, Vol. 47, pp. 425-449, 2011.
- [4] Reding P and Jecmen D. Effects of external burning on spike-induced separated flow *Journal of Spacecraft*, Vol. 20, No. 5, pp. 452-453, 1983.
- [5] Jiang Z, Liu Y, Han G and Zhao W. Experimental demonstration of a new concept of drag reduction and thermal protection for hypersonic vehicles. *Acta Mech Sin*, Vol. 25, pp. 417-419, 2009.
- [6] Tamada I, Aso S and Tani Y. Numerical study of the effect of the opposing jet on reduction of aerodynamic heating with different nose configurations. *Proc 26th International Council of the Aeronautical Sciences*, Anchorage, USA, 2008.
- [7] McBride B and Gordon S. Computer program for calculation of complex chemical equilibrium compositions and applications; II. user's manual and program description. NASA RP-1311, 1996.
- [8] Lordi J, Mate R and Moselle J. Computer program for the numerical solution of nonequi-

librium expansions of reacting gas mixtures. NASA CR-472, 1966.

- [9] Billig F. Shock-wave shapes around spherical- and cylindrical-nosed bodies. *Journal of Spacecraft*, Vol. No. 6, pp. 822-823, 1967.
- [10] Edney B. Anomalous heat transfer and pressure distributions on blunt bodies at hypersonic speeds in the presence of an impinging shock. FAA Report-115, The Aeronautical Research Institute of Sweden, 1968.

Contact Author Email Address

mailto: morimoto@aero.kyushu-u.ac.jp

Copyright Statement

The authors confirm that they, and/or their company or organization, hold copyright on all of the original material included in this paper. The authors also confirm that they have obtained permission, from the copyright holder of any third party material included in this paper, to publish it as part of their paper. The authors confirm that they give permission, or have obtained permission from the copyright holder of this paper, for the publication and distribution of this paper as part of the ICAS 2014 proceedings or as individual off-prints from the proceedings.